

Nonlinear stopping power of an electron gas for slow ions

P. M. Echenique*

Cavendish Laboratory, Cambridge, CB3 0HE, England

R. M. Nieminen

Department of Physics, University of Jyväskylä, SF-40100 Jyväskylä 10, Finland

J. C. Ashley and R. H. Ritchie

Health and Safety Research Division, Oak Ridge National Laboratory, Oak Ridge, Tennessee 37831

(Received 20 June 1985)

Theoretical calculations of the stopping power of the electron gas for slow ions, $v < v_F$, are reviewed. New results are presented for stopping power and effective charge based on nonlinear density-functional calculations. Extensive comparisons with available experimental data show that these new theoretical results are clearly superior to earlier calculations based on linear theory.

INTRODUCTION

The problem of energy losses suffered by energetic ions moving in condensed matter is one of continuing interest in physics. When the ion velocity is greater than the average velocity of valence electrons in solids, a good description of the loss process can be achieved using a linear-response theory to calculate the loss due to the valence-band electrons together with atomic-type calculations to evaluate the effect of losses due to core-electron excitations.

The case of ions traveling with velocities smaller than the Fermi velocity of the electron gas is of special interest in cases such as the slowing and reflection of hydrogen atoms impinging on the inner wall of a controlled thermonuclear reactor.¹ Oen and Robinson² have estimated, using Monte Carlo methods, the number and energy of atoms reflected from a metal surface. Following the pioneering work of Fermi and Teller,³ some calculations were done within the framework of linear-response theory. An attempt to include the effect of an electron bound to the projectile was performed by Ferrell and Ritchie.⁴ The first nonlinear calculation in the static limit was performed by Echenique, Nieminen, and Ritchie⁵ using density-functional formalism to calculate the response of the electron gas to the perturbation produced by the incoming ion. The density-functional formalism has proven to be a very useful tool in calculating many atomic and electronic processes similar to the stopping power such as the impurity resistivity⁶ and the damping rate of a vibrating atom on a metal surface.⁷ Phase shifts and cross sections related to these problems have been calculated by a number of authors.⁸⁻¹⁰ In this paper we present a detailed analysis of the density-functional results and comparisons with experimental data, as well as predictions of the stopping power for media for which no experimental data are available. An extension of the results for protons⁵ to higher charge is also included, showing in a natural way the “ Z_1 oscillation.” We begin with a description of the linear-response theory and the Ferrell-

Ritchie theory to put the density-functional results in their proper perspective.

THEORY OF ELECTRON-GAS STOPPING POWER

Fermi and Teller³ were the first to report a calculation of the energy loss per unit path length of a slow, charged particle moving with velocity v much less than the Fermi velocity v_F . They were interested in seeing if the intrinsic lifetime of a muon (with $v \ll v_F$) is comparable to the time required for it to slow to rest in the medium. By arguing that due to the exclusion principle only electrons within a small range v just under the Fermi surface will participate in the loss process, they found the energy loss of a muon per unit distance traversed in the medium to be

$$\frac{dW}{dR} = \left[\frac{2v}{3\pi} \right] \ln \left[\frac{1}{\alpha r_s} \right], \quad (1)$$

where $\alpha = (4/9\pi)^{1/3}$, $r_s = (3/4\pi n)^{1/3}$ is the “one-electron radius” (the radius of a sphere containing, on average, one electron), and n is the electron density. We use Hartree atomic units, in which $e = \hbar = m = 1$, throughout this paper. In linear-response theory the stopping power of a medium for a charged particle, with charge Z_1 , is given by

$$\frac{dW}{dR} = \frac{2Z_1^2}{\pi v^2} \int_0^\infty \omega d\omega \int_{\omega/v}^\infty \frac{dk}{k} \text{Im} \left[-\frac{1}{\epsilon(k, \omega)} \right], \quad (2)$$

where $\epsilon(k, \omega)$ is the longitudinal dielectric function for the stopping medium. For high velocities a classical dielectric function can be used

$$\epsilon(k, \omega) \rightarrow \epsilon(\omega) = 1 - \frac{\omega_p^2}{\omega(\omega + i\gamma)}, \quad (3)$$

where γ is a positive infinitesimal and ω_p is the electron-gas plasma frequency, $\omega_p = (3/r_s^3)^{1/2}$. This leads to an expression having the general form of Bethe’s result¹¹ for

the stopping power of an electronic system for the charged particle given by

$$\frac{dW}{dR} = Z_1^2 \frac{\omega_p^2}{v^2} \ln \left(\frac{2v^2}{\omega_p} \right). \quad (4)$$

For high-velocity ions, $v \gg v_F$, an oscillatory wake¹² trails the ion. These oscillations constitute an important mode of energy loss for swift protons and are related to many interesting phenomena.¹² However, we shall restrict our attention here to the case of slow ions. At low velocities ($v \ll v_F$) an improvement over the Fermi-Teller formula can be obtained using, in Eq. (2), the full random-phase approximation (RPA) for ϵ .¹³ An expression was obtained by Ritchie¹⁴ using an approximation to the RPA dielectric function valid for small ω and $k \leq k_F$, where k_F is the Fermi momentum. This is equivalent to assuming that the potential around an ion is exponentially screened by density fluctuations in the electron gas. The result is

$$\frac{dW}{dR} = Z_1^2 \left(\frac{2v}{3\pi} \right) \left[\ln \left(1 + \frac{\pi}{\alpha r_s} \right) - \frac{1}{1 + \alpha r_s / \pi} \right]. \quad (5)$$

The results for $(1/v)(dW/dR)$ in linear-response theory using the RPA dielectric function together with the results of Fermi and Teller [Eq. (1)] and Ritchie [Eq. (5)] are shown in Fig. 1. Figure 2 shows the linear-response calculation for the variation of dW/dR for a proton with velocity v in an electron gas of a density equal to that of aluminum. The total is computed from Eq. (2) using the RPA dielectric function.¹³ The contribution of the plasmons, which give rise to the wake for $v \gg v_F$, is shown separately in the figure. Experimental data are shown as dots in this figure and were taken from the work of Young.¹⁵ Ferrell and Ritchie⁴ calculated the stopping power of an electron gas for slow, singly ionized He atoms in linear-response theory using a wave function for the bound electron determined self-consistently in the electron gas. The stopping power is then

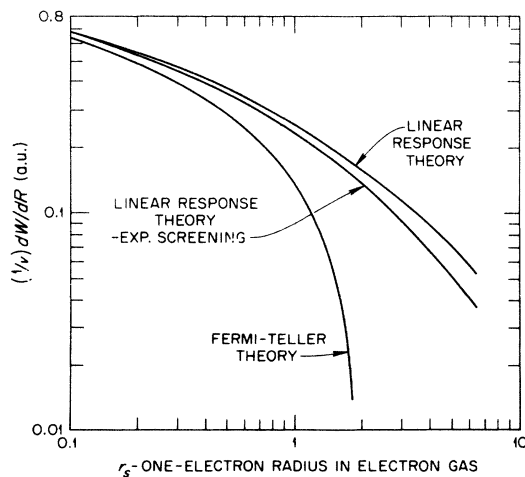


FIG. 1. Comparison of calculations of stopping power of an electron gas for a slow proton in the form $(1/v)(dW/dR)$ versus the one-electron radius r_s .

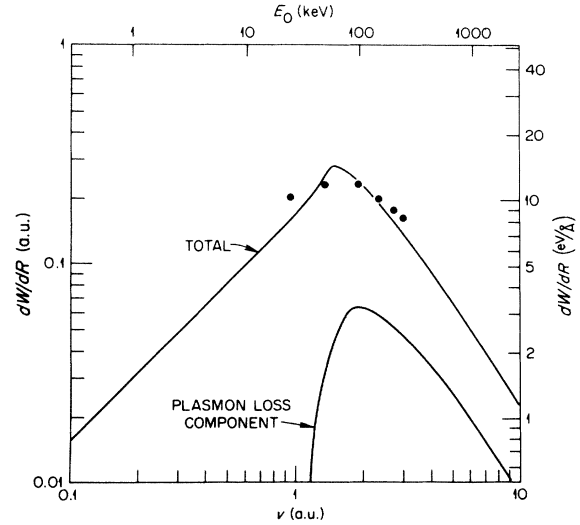


FIG. 2. The stopping power of an electron gas with $r_s = 2.07$ (corresponding to aluminum) for a proton of speed v . The contribution of plasmon excitation to the energy loss per unit path length of the proton is also shown. The dots show experimental data from Ref. 15.

$$\frac{dW}{dR} = \frac{1}{4\pi^4 v} \int \frac{d\mathbf{k}}{k^2} F(k^2) \int_0^\infty \omega d\omega \operatorname{Im} \left[-\frac{1}{\epsilon(k, \omega)} \right] \times \delta(\omega - \mathbf{k} \cdot \mathbf{v}), \quad (6)$$

with $F(k^2)$ given by

$$F(k^2) = 4\pi^2 \left[Z_1 - \int d\mathbf{r}' e^{i\mathbf{k} \cdot \mathbf{r}'} |U(\mathbf{r}')|^2 \right]^2. \quad (7)$$

A hydrogenic wave function $U(r) = (a^3/\pi)^{1/2} e^{-ar}$ is employed, with the parameter a determined variationally by minimizing the total energy of the ion plus a bound electron in the electron gas.

An improvement over the linear-theory result can be achieved using Feynman-diagram methods. Including the effect of the Pauli principle by restricting electron states to those outside the occupied Fermi sphere only in the last transition, one finds^{4,16} for the stopping power

$$\frac{dW}{dR} = vv_F n_0 \sigma_{tr}, \quad (8)$$

where σ_{tr} is the usual transport cross section. In terms of the scattering cross section σ , σ_{tr} is given by

$$\begin{aligned} \sigma_{tr} &= \int d\sigma (1 - \cos\theta) \\ &= \frac{4\pi}{k_F^2} \sum_{l=0}^{\infty} (l+1) \sin^2(\delta_l - \delta_{l+1}), \end{aligned} \quad (9)$$

where θ is a scattering angle in the proton's frame and δ_l is the phase shift of the l th partial wave for scattering of electrons at the Fermi surface from the screened potential of the proton. A similar analysis was used by Josephson and Lekner¹⁷ to study the scattering of ions by ³He quasiparticles.

EFFECTIVE CHARGE

Brandt¹⁸ was able to condense a great amount of data by introducing the concept of effective charge. An ion of charge Z_1 will move in a medium accompanied by a cloud of bound electrons consisting of $N_1(v_r)$ electrons extending over a radius $\Lambda(v_r)$, where v_r is the ion-electron relative speed. In Brandt's approach, electrons in the medium at impact parameter larger than Λ encounter the ion as a point charge $Q_1(v_r) = Z_1 - N_1(v_r)$ in distant collisions, but a larger ionic charge than Q_1 for smaller impact parameters. On averaging over all impact parameters, the effective charge $Z_1^*(v_r)$ of the ion of given Q_1 that is appropriate for the stopping power of the medium is therefore always larger than $Q_1(v_r)$. This method has provided much physical insight, and has allowed the condensing of a great amount of otherwise dispersed experimental data. In this paper we shall be working within a nonlinear framework in which the bound states of the ion will appear in a natural way, making it unnecessary to relate the effective charge to the mean ionic charge. In fact, the mean ionic charge is sometimes zero because all bound states are occupied. Thus we take another definition for the effective charge, defining it in an operational manner as

$$Z_1^* = \left[\left[\frac{dW}{dR} \right]_{Z_1} / \left[\frac{dW}{dR} \right]_1 \right]^{1/2}. \quad (10)$$

DENSITY-FUNCTIONAL CALCULATION

For low ion velocities the physics of the ion-electron-gas interaction occurs via scattering at the Fermi surface and can be codified in phase shifts at the Fermi energy leading to scattering cross sections and energy loss. Electrons at the Fermi surface are viewed as being scattered by the screened potential of the ion. The stopping power for a slow ion can then be written^{4,16} as

$$\frac{dW}{dR} = \frac{3v}{k_F r_s^3} \sum_{l=0}^{\infty} (l+1) \sin^2[\delta_l(E_F) - \delta_{l+1}(E_F)], \quad (11)$$

where $\delta_l(E_F)$ are the phase shifts at the Fermi energy for scattering of an electron off a spherically symmetric, self-consistent potential. Since the ion is moving slowly compared with the electrons at the Fermi surface, we can use the results of a static calculation for such a potential.

Ferrell and Ritchie⁴ used Eq. (11) to calculate the stopping power assuming a linear-response, Yukawa-type potential for the ion-electron interaction potential

$$V(r) = Z_1 \frac{e^{-\kappa r}}{r}, \quad (12)$$

with $\kappa = 3\alpha/r_s^{1/2}$. Work by Almbladh *et al.*⁸ and others shows that the results of nonlinear density-functional calculations for the density fluctuations and induced potentials of a static proton in an electron gas differ substantially from the ones obtained from linear-response theory.

The ratios of the induced electron density calculated in the nonlinear theory to the results obtained in the linear theory using the random-phase approximation¹⁹ vary over the range of metallic densities from 1.93 for $r_s = 1$ to 33.7

for $r_s = 6$. This last number is within 10% of the ones which will be obtained from the $1s$ atomic orbital, showing as they should the atomic nature of the bound state in a dilute electron gas. These results prove that, for low ion velocities, linear response does not describe adequately the scattering process and one has to go beyond it to calculate correctly the stopping power.

We have used the density-functional formulation of Hohenberg and Kohn, and Kohn and Sham²⁰ to calculate the self-consistent potential due to a static charge submerged in an electron gas at metallic densities. In the density-functional method one writes for the one-electron Schrödinger equation

$$\left[-\frac{\nabla^2}{2} + V(\mathbf{r}) + v^{xc}(\mathbf{r}) \right] \Psi_i(\mathbf{r}) = E_i \Psi_i(\mathbf{r}), \quad (13)$$

which yields the electron density

$$\rho(\mathbf{r}) = \sum_i |\Psi_i(\mathbf{r})|^2. \quad (14)$$

The potential V is that seen by an electron as a result of the nonlinear screening of the ion by the electron gas. The screening charge is composed of two parts, a bound-state component and a contribution from scattering states. The exchange and correlation potential $v^{xc}(\mathbf{r})$ is a local potential depending on the total density $\rho(\mathbf{r})$. The sum in Eq. (14) is over electron states in the gas. We have only dealt with spin-compensated systems in our calculations, although the results could be easily extended in a straightforward manner to magnetic systems. The local-density approximation for exchange and correlation has been used with the parametrization given by Gunnarsson and Lundqvist.²¹

Equations (13) and (14) are solved self-consistently to get the charge density and the phase shifts for the conduction band as a function of the energy. The scattering phase shifts at the Fermi energy due to the complete screening of the nuclear charge will satisfy the Friedel sum rule⁶

$$Z_1 = \frac{2}{\pi} \sum_l (2l+1) \delta_l(E_F). \quad (15)$$

The calculated phase shifts satisfy the Friedel sum rule for all energies to a good accuracy, usually within 0.02 electrons.

RESULTS

Hydrogen and helium projectiles

In their brief report Echenique, Nieminen, and Ritchie⁵ compared the results for H and He with the ones obtained by linear-response theory and by the method of Ferrell and Ritchie.⁴ For completeness we reproduce those results together with a detailed comparison with experimental data^{22,23} and predictions of stopping powers for protons and α particles in solids for which no reliable experimental data are available.

In Fig. 3 we show the comparison of the density-functional results with the ones obtained by linear theory and the method of Ferrell and Ritchie. Curve A was cal-

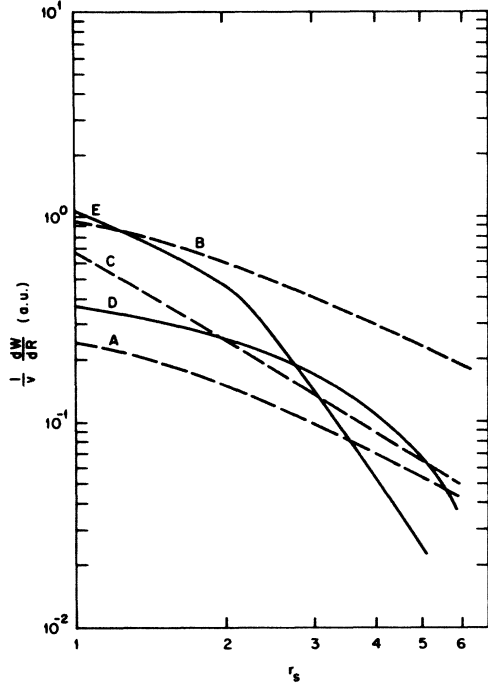


FIG. 3. Stopping powers as functions of r_s . Curve A is calculated in linear-response theory, Eq. (5), for $Z_1=1$; curve B from Eq. (5) with $Z_1=2$. Curve C is the result from Ref. 4 for a slow, singly ionized He atom. Curves D and E are the density-functional results for a proton and a helium nucleus, respectively. In all cases $v \ll v_F$.

culated in linear-response theory, from Eq. (5) for $Z_1=1$, while curve B was computed from the same equation for $Z_1=2$. We show in curve C the results of the calculation by Ferrell and Ritchie⁴ of the stopping power for a slow, singly ionized He atom calculated from linear-response theory using a wave function for the bound electron determined self-consistently in the electron gas. Curves D and E were computed from the density-functional approach for a proton and a He nucleus, respectively. At metallic densities a doubly occupied bound state exists below the bottom of the conduction band. As r_s decreases toward values much less than 1, our results tend toward agreement with linear theory, that is, all stopping powers tend to be proportional to Z_1^2 . This is easily visualized when one considers that for large electron-gas densities the screening of the ion is so strong that bound states cannot exist; thus the electrons are scattered essentially by an exponentially screened potential with screening length approaching zero as r_s goes to zero. It is interesting to note that for $r_s < 1.2$, curve E, computed for a He nucleus, actually lies above curve B, computed from Eq. (5) taking $Z_1=2$.

As r_s increases, the energy loss for both H and He decreases more rapidly than predicted by linear theory due to the fact that bound states of atomic character develop, thereby tending to screen out interactions with the electron gas. The energy loss of a He nucleus at large r_s is smaller than that of a proton at the same velocity. This is qualitatively different from any linear theory in which the

energy loss scales as the square of the ionic charge and can be easily understood in terms of the atomic character of the scattering process in a very dilute electron gas. This shows very clearly if we calculate the effective charge as a function of r_s for a He nucleus. In Fig. 4 we show the results of such a calculation. The effective charge, Eq. (10), varies from $Z_1^*=2$ for $r_s \rightarrow 0$ to 0.46 for $r_s=6$. It becomes less than 1 for $r_s \gtrsim 2.7$.

We show for protons the comparison between the density-functional results and the ones obtained with the commonly used Lindhard and Winther (LW) equation.²⁴ In the latter approach, which does not go beyond linear response, the low-velocity stopping power is given by

$$\left[\frac{1}{v} \frac{dW}{dR} \right]_{LW} = \frac{2Z_1^2}{3\pi} \left[\ln \left[\frac{1+2\chi^2/3}{\chi^2} \right] - \frac{1-\chi^2/3}{1+2\chi^2/3} \right] \times (1-\chi^2/3)^{-2}, \quad (16)$$

where $\chi^2=0.166r_s$. This form is a very good approximation to the values predicted numerically by using the exact RPA dielectric response function for an electron gas in Eq. (2). The dramatic increase of the nonlinear, density-functional results over those of the linear-response theory is clearly shown in Fig. 5 for $Z_1=1$. For many solids used in experiments ($1.5 \leq r_s \leq 2.5$) the density-functional results show increases of $\sim 65\%$ over the Lindhard-Winther predictions.

A comparison of experimental data with the density-functional predictions for protons using the results of Echenique, Nieminen, and Ritchie⁵ (ENR) was made by Mann and Brandt.²² They collected data on targets covering a wide range of atomic numbers and plotted reduced stopping powers

$$\left[\frac{1}{v_F} \frac{dW}{dR} \right] / \left[\frac{1}{v} \frac{dW}{dR} \right]_{LW}$$

as a function of v/v_F , where v_F is the Fermi velocity.

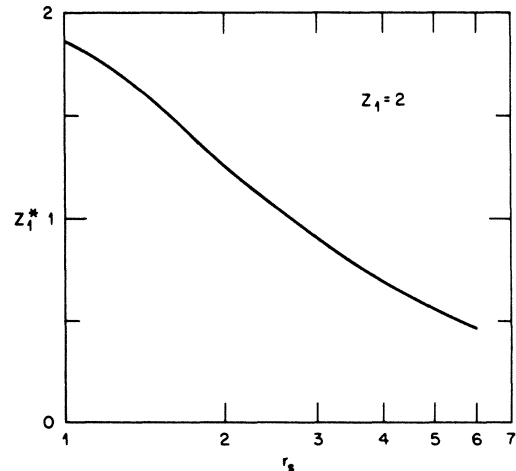


FIG. 4. Effective charge, Eq. (10), for a He nucleus as a function of r_s , calculated using the density-functional approach.

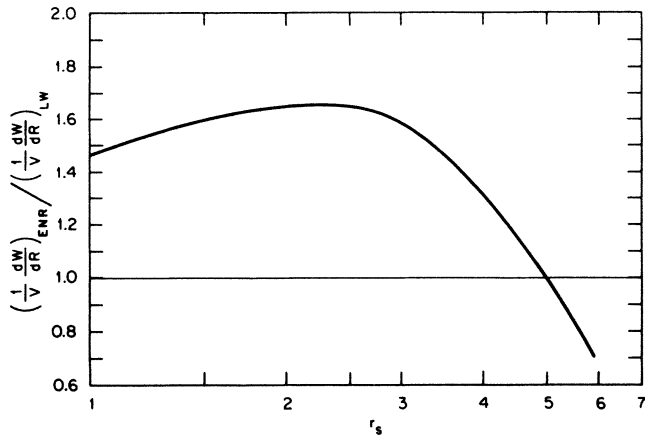


FIG. 5. Comparison of the stopping power for a proton calculated using the density-functional approach to the Lindhard-Winther predictions of Eq. (16).

The values of r_s were taken from Isaacson's tables.²⁵ Their comparisons are shown in Fig. 6 with the density-functional results given by the curve labeled ENR and the Lindhard-Winther prediction labeled LW. The curve labeled FR is the theoretical prediction by Ferrell and Ritchie as described above. As a guide to the comparison of data with theory, short-dashed lines are included giving a $\pm 15\%$ variation around the line ENR. The generic data shown in the figure, described in detail in Ref. 22, represent values for 20 different elemental solids in the

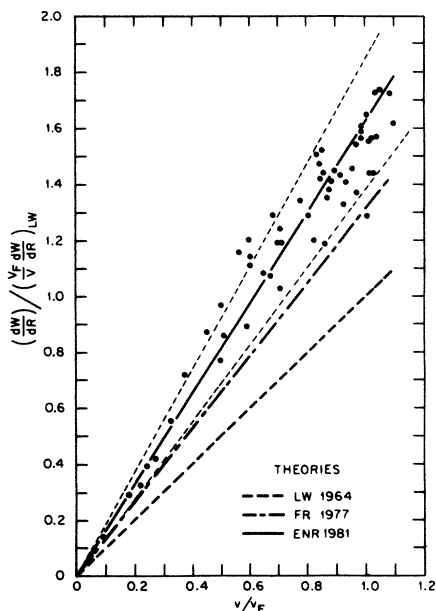


FIG. 6. Comparisons of theoretical stopping powers for protons with experimental data. The curve LW is the Lindhard-Winther prediction (Ref. 24) calculated from Eq. (16); FR is the Ferrell-Ritchie prediction from Ref. 4; ENR is the density-functional result from Ref. 5. The short-dashed lines give a $\pm 15\%$ variation about the line ENR. Reference 22 gives the identity of, and sources for, the generic data shown as solid circles in the figure.

range $4 \leq Z_2 \leq 83$. Mann and Brandt conclude from these comparisons that within the uncertainties of the data (1) the density-functional predictions give good agreement with the data, and (2) the linear dependence on velocity holds up to $v \approx v_F$.

Additional comparisons of theory and experiment may be made²³ using results compiled by Andersen and Ziegler²⁶ in a book on stopping powers. They collected experimental data for a wide range of energies and employed simple analytic forms to obtain a "best-fit" for several elemental solids. For energies below 10 keV, a simple, velocity-proportional expression for stopping power is given. These data-based fits are compared with the density-functional results as stopping-power ratios. The ratios are shown as solid circles in Fig. 7 for 16 elemental solids specified by their atomic number Z_2 . With the exception of Pb ($Z_2=82$) the agreement is similar to that of Fig. 6. Andersen and Ziegler used an interpolation scheme (described in Ref. 26) to predict stopping powers of materials for which no data were available. Comparisons for several solids are shown as x's in Fig. 7. Substantial variations about the density-functional predictions are seen for these less-reliable estimates.

Ions with $Z_1 > 2$

We have extended our work to ions with $Z_1 > 2$ using the density-functional approach. For most charges and electron densities, self-consistency was achieved. In Fig. 8 we show the effective charge defined by Eq. (10) for several incident bare ions and for three electron-gas densities. For $r_s=4$, self-consistency in the calculations was not obtained for $Z_1=15$ and 16. This gap is indicated by the light, dashed line in Fig. 8. The Z_1 oscillations appear naturally since they are related to the appearance of new bound states which are taken into account in a natural way in our self-consistent calculation. A qualitative understanding of the main features of the oscillation can easily be achieved in terms of scattering theory and resonance levels in solids, since the problem is analogous to the residual resistivity due to nonmagnetic impurities in

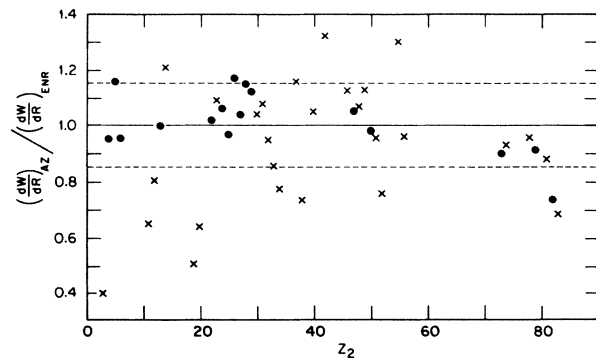


FIG. 7. Ratios of stopping powers for low-velocity protons from Anderson and Ziegler (AZ) (Ref. 26), $(dW/dR)_{AZ}$, to the density-functional predictions of Ref. 5, $(dW/dR)_{ENR}$. The solid circles represent experimental data for 16 elemental solids, while the crosses are interpolations to materials for which no experimental data are available.

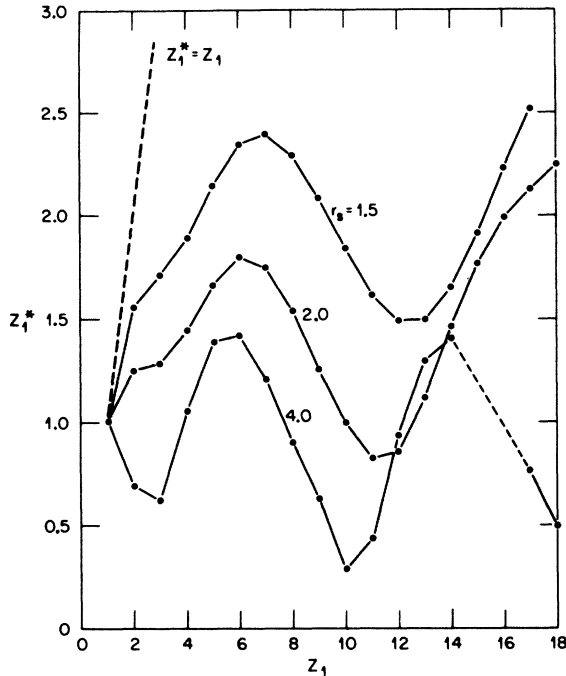


FIG. 8. Effective charge Z_1^* , defined by Eq. (10), as a function of Z_1 for $r_s = 1.5, 2$, and 4 .

solids.⁶ For small charge, doubly occupied bound states are found in the density-functional calculation. For $Z_1 = 5-8$ the $2p$ electrons form an unbound, resonant state in the conduction band. That this will produce a maximum in the scattering cross section can be easily understood by taking into account the resonant phase shifts, approximating them from the Friedel sum rule as

$$\delta_1 \cong \frac{\pi(Z_1 - 4)}{6}. \quad (17)$$

This will predict a maximum in the stopping power when $\delta_1 = \pi/2$ thus at $Z_1 = 7$. Similar arguments explain qualitatively the oscillating structure of the curves as maxima due to $3p$, $3d$, and $4p$ resonances, while minima are related to the formation of closed shells. For a dilute electron gas the screening cloud approaches the free-atom electron structure, and the minima appear at the formation of closed atomic shells as the screening increases due to increasing electronic density. This minimum shifts to higher ionic charges since a stronger ionic potential is necessary to compensate the electronic screening and so have the strength to bind an extra electron. This is clearly shown in the graph as displacement of the minimum from the atomic value ($Z_1 = 10$) as the electron density increases (r_s decreases). For very small r_s , no bound states are formed and linear-response theory should be valid, and Z_1^* approaches Z_1 . For the values of Z_1 shown in Fig. 8, the ratio of maximum to minimum values in the stopping power decreases from 25 for $r_s = 4$ to 2.6 for $r_s = 1.5$. The slope of the effective charge as a function of Z_1 changes sign at $r_s \sim 3$ for $Z_1 \leq 3$ as r_s increases. This

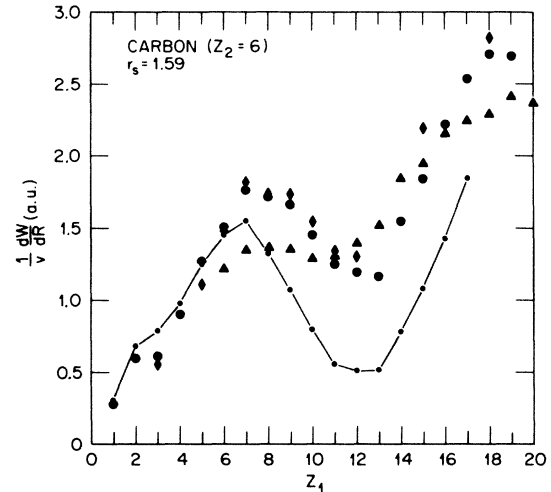


FIG. 9. Stopping power of carbon as a function of Z_1 . The density of carbon is taken to be 2 g cm^{-3} . The chained curve gives the theoretical predictions for $r_s = 1.59$. The sources of the experimental data are \bullet , Ref. 27; \blacktriangle , Ref. 28; \blacklozenge , Ref. 29.

was explained in the analysis of the He versus H results. Comparisons of experimental data with the theoretical predictions for stopping power of carbon and aluminum are shown in Figs. 9 and 10 for $1 \leq Z_1 \leq 20$. For carbon we assume a density $\rho = 2 \text{ g cm}^{-3}$ and four electrons per carbon atom to produce an electron gas with $r_s = 1.59$. The theoretical predictions for $(1/v)(dW/dR)$, in atomic units, are shown in Fig. 9 as a function of Z_1 with line segments between the points as a visual guide. The experimental data are from Ref. 27 for $v = 0.411$, solid dots, Ref. 28 for $v = 0.826$, triangles, and Ref. 29 for $v = 0.25$, diamonds. The data and theory show the same overall trends with good quantitative agreement for $Z_1 \leq 7$. For aluminum targets, Fig. 10, the overall trends of theory and experiment are similar but with substantial disagree-

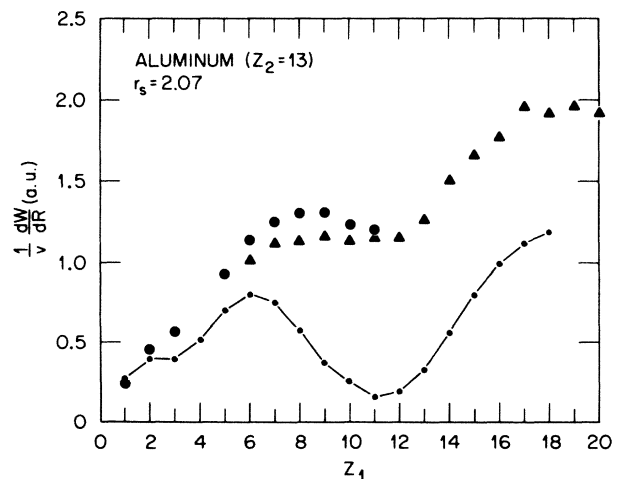


FIG. 10. Stopping power of aluminum as a function of Z_1 . The chained curve gives the theoretical predictions for $r_s = 2.07$. The sources of the experimental data are \bullet , Ref. 27; \blacktriangle , Ref. 28.

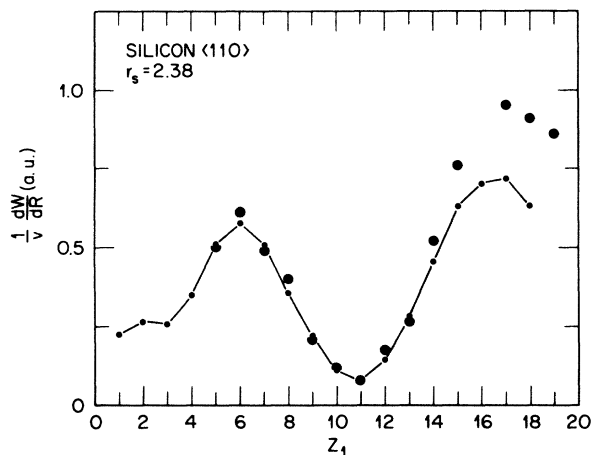


FIG. 11. Stopping power for "well-channeled" ions in the $\langle 110 \rangle$ axial channel of silicon as a function of Z_1 . The chained curve gives the theoretical predictions for $r_s=2.38$. The experimental points are from Ref. 30.

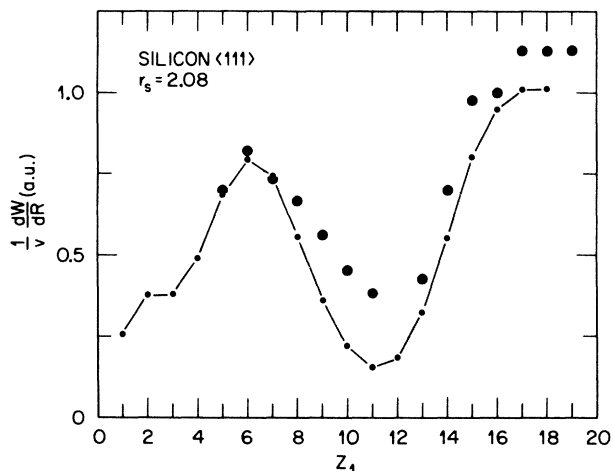


FIG. 12. Stopping power for "well-channeled" ions in the $\langle 111 \rangle$ axial channel of silicon as a function of Z_1 . The chained curve gives the theoretical predictions for $r_s=2.08$. The experimental points are from Ref. 31.

ment in magnitude, particularly around the minimum at $Z_1=11$. The experimental data for aluminum are from Ref. 27 for $\nu=0.411$, solid dots, and Ref. 28 for $\nu=0.826$, triangles.

Additional comparisons can be made with Eisen's data^{30,31} on the energy loss of "best-channeled" ions in the $\langle 110 \rangle$ and $\langle 111 \rangle$ axial channels in Si. The electron density in a channel increases from a small value along the axis to values an order of magnitude larger near the strings of atoms defining the channel. This density variation is well characterized for the $\langle 110 \rangle$ axial channel in Si.³² Since a range of electron densities (or impact parameters) is sampled in the energy-loss process, we will make our comparisons with the data using an average electron-gas density determined by making theoretical and experimental values equal at $Z_1=5$. These comparisons are shown in Figs. 11 and 12. For the $\langle 110 \rangle$ channel we have $r_s=2.38$ and for the $\langle 111 \rangle$ channel, $r_s=2.08$. As expected, these values correspond to lower densities than the average valence-electron density (corresponding to $r_s=2.0$). In both figures the overall trends in the data are closely reproduced by the theoretical calculations.

CONCLUSIONS

We have reviewed earlier linear theory and presented new results for the energy loss of slow ions in an electron gas. Variations of stopping power with incident ion charge, the Z_1 oscillations, arise in a natural way in the nonlinear theory, while such oscillations are not expected to arise³³ from Brandt's effective-charge theory.¹⁸ The comparisons of these new results with experimental data emphasize the need to employ a nonlinear theory in studies of slow-ion interactions with solids.

ACKNOWLEDGMENTS

This research sponsored jointly by the U.S.—Spain Joint Committee for Scientific and Technological Cooperation, under Grant No. IAG 40-1516-84, and the Office of Health and Environmental Research, U.S. Department of Energy, under Contract No. DE-AC05-84OR21400 with Martin Marietta Energy Systems, Inc. One of the authors (P.M.E.) gratefully acknowledges help and support from Iberduero S. A. and the March Foundation.

*On leave from Euskal Herriko Unibertsitatea, Quimicas, Donostia, Euzkadi (The Basque Country).

¹J. T. Hogan and J. F. Clarke, *J. Nucl. Mater.* **53**, 1 (1974).

²O. S. Oen and M. T. Robinson, *Nucl. Instrum. Methods* **132**, 647 (1976).

³E. Fermi and E. Teller, *Phys. Rev.* **72**, 399 (1947).

⁴L. Ferrell and R. H. Ritchie, *Phys. Rev. B* **16**, 115 (1977).

⁵P. M. Echenique, R. M. Nieminen, and R. H. Ritchie, *Solid State Commun.* **37**, 779 (1981).

⁶C. Kittel, *Quantum Theory of Solids* (Wiley, New York, 1963).

⁷M. Persson and B. Hellsing, *Phys. Rev. Lett.* **49**, 662 (1982).

⁸C. O. Almbladh, U. von Barth, Z. D. Popovic, and M. J. Stott,

Phys. Rev. B **14**, 2250 (1976).

⁹P. Jena and K. S. Singwi, *Phys. Rev. B* **17**, 3518 (1978).

¹⁰M. J. Puska and R. M. Nieminen, *Phys. Rev. B* **27**, 6121 (1983).

¹¹H. A. Bethe, *Ann. Phys. (N.Y.)* **5**, 325 (1930).

¹²J. Neufeld and R. H. Ritchie, *Phys. Rev.* **98**, 1632 (1955); V. N. Neelavathi, R. H. Ritchie, and W. Brandt, *Phys. Rev. Lett.* **33**, 302 (1974); **33**, 670(E) (1974); **34**, 560(E) (1975); P. M. Echenique, R. H. Ritchie, and W. Brandt, *Phys. Rev. B* **20**, 2567 (1979).

¹³J. Lindhard, *K. Dan. Vidensk. Selsk. Mat. Fys. Medd.* **28**, No. 8 (1954).

- ¹⁴R. H. Ritchie, *Phys. Rev.* **114**, 644 (1959).
- ¹⁵J. R. Young, *J. Appl. Phys.* **27**, 1 (1956).
- ¹⁶J. Finneman, Ph.D. dissertation, The Institute of Physics, Aarhus University, 1968 (unpublished); N. F. Mott and H. Jones, *The Theory and Properties of Metals and Alloys* (Dover, New York, 1958), p. 294, employ this model in the Born approximation to estimate the contribution of impurity scattering to the resistivity of metals.
- ¹⁷B. D. Josephson and J. Lekner, *Phys. Rev. Lett.* **23**, 111 (1969).
- ¹⁸W. Brandt, in *Atomic Collisions in Solids*, edited by S. Datz, B. R. Appleton, and C. D. Moak (Plenum, New York, 1975), Vol. 1, p. 261; W. Brandt, *Nucl. Instrum. Methods* **194**, 13 (1982).
- ¹⁹J. S. Langer and S. H. Vosko, *J. Phys. Chem. Solids* **12**, 196 (1960); see also A. Mazarro, P. M. Echenique, and R. H. Ritchie, *Phys. Rev. B* **27**, 4117 (1983).
- ²⁰P. Hohenberg and W. Kohn, *Phys. Rev. B* **136**, 964 (1964); W. Kohn and L. J. Sham, *Phys. Rev. A* **140**, 1133 (1965).
- ²¹O. Gunnarsson and B. I. Lundqvist, *Phys. Rev. B* **13**, 4274 (1976).
- ²²A. Mann and W. Brandt, *Phys. Rev. B* **24**, 4999 (1981).
- ²³J. C. Ashley and R. H. Ritchie, Oak Ridge National Laboratory Report No. CONF 8404190, 1985, pp. 266–271 [available from National Technical Information Service (NTIS), U.S. Department of Commerce, 5285 Port Royal Road, Springfield, VA 22161. NTIS price codes—printed copy: A19; microfiche: A01].
- ²⁴J. Lindhard and A. Winther, *K. Dan. Vidensk. Selsk. Mat. Fys. Medd.* **34**, No. 4 (1964).
- ²⁵D. Isaacson, New York University Document No. 02698 (National Auxiliary Publication Service, New York, 1975).
- ²⁶H. H. Andersen and J. F. Ziegler, *Hydrogen Stopping Powers and Ranges in All Elements* (Pergamon, New York, 1977).
- ²⁷J. H. Ormrod and H. E. Duckworth, *Can. J. Phys.* **41**, 1424 (1963); J. H. Ormrod, J. R. Macdonald, and H. E. Duckworth, *ibid.* **43**, 275 (1965).
- ²⁸D. Ward, H. R. Andrews, I. V. Mitchell, W. N. Lennard, R. E. Walker, and N. Rud, *Can. J. Phys.* **57**, 645 (1979).
- ²⁹G. Högberg, *Phys. Status Solidi B* **46**, 829 (1971).
- ³⁰F. H. Eisen, *Can. J. Phys.* **46**, 561 (1968).
- ³¹J. S. Briggs and A. P. Pathak, *J. Phys. C* **7**, 1929 (1974), display F. H. Eisen's previously unpublished data for the $\langle 111 \rangle$ channel in Si.
- ³²J. A. Golovchenko, D. E. Cox, and A. N. Goland, *Phys. Rev. B* **26**, 2335 (1982).
- ³³N. Barberan and P. M. Echenique (unpublished).